Preclinical safety and efficacy studies with an affinity-enhanced epithelial junction opener and PEGylated liposomal doxorubicin.

Maximilian Richter, Roma Yumul, Hongjie Wang, Kamola Saydaminova, Martin Ho, Drew May, Audrey Baldessari, Michael Gough, Charles Drescher, Nicole Urban, et al.

Citation: Molecular Therapy — Methods & Clinical Development (2015) **2,** 15005; doi:10.1038/mtm.2015.5

www.nature.com/mtm

ARTICLE

Preclinical safety and efficacy studies with an affinity-enhanced epithelial junction opener and PEGylated liposomal doxorubicin

Maximilian Richter[1], Roma Yumul[1], Hongjie Wang[1], Kamola Saydaminova[1], Martin Ho[1], Drew May[2], Audrey Baldessari[2], Michael Gough[2], Charles Drescher[3], Nicole Urban[3], Steve Roffler[4], Chloé Zubieta[5], Darrick Carter[1,6], Pascal Fender[7] and André Lieber[1,8]

A central treatment resistance mechanism in solid tumors is the maintenance of epithelial junctions between malignant cells that prevent drug penetration into the tumor. We have developed a small recombinant protein (JO-1) that triggers the transient opening of intercellular junctions and thus increases the efficacy of monoclonal antibodies and chemotherapeutic drugs without causing toxicity in mouse tumor models. Here, we provide data toward the clinical translation of an affinity-enhanced version of JO-1, which we call JO-4, in combination with PEGylated liposomal doxorubicin (PLD)/Doxil for ovarian cancer therapy. We have presented X-ray crystallography data suggesting a structural basis for the higher affinity of JO-4 to DSG2. We also confirmed JO-4 efficacy in a xenograft model with primary ovarian cancer cells showing that JO-4 can salvage Doxil therapy when given at a dose that was threefold lower than the therapeutic dose. Furthermore, we tested the safety of intravenous JO-4 alone and in combination with Doxil in *Macaca fascicularis*, an adequate animal model for predicting toxicity in humans. Our studies did not show critical JO-4-related toxicity or an increase of Doxil-related side effects. Our efficacy and safety data will help to support an Investigational new drug-filing for a JO-4/Doxil combination treatment.

Molecular Therapy — Methods & Clinical Development (2015) **2**, 15005; doi:10.1038/mtm.2015.5; published online 11 March 2015

INTRODUCTION

Epithelial phenotype of cancer

More than 80% of all cancer cases are carcinomas, formed by the malignant transformation of epithelial cells. One of the key features of epithelial tumors is the presence of intercellular junctions, which link cells to one another and act as barriers to the penetration of molecules with a molecular weight of >400 daltons (Da).[1–3] One of these junction proteins, desmoglein 2 (DSG2), is upregulated in malignant cells.[4,5] For example, in more than 60 ovarian cancer biopsies with different histological types analyzed, we consistently found higher expression levels of DSG2 in ovarian cancer cells than in the surrounding normal tissue or tumor stroma cells.[6]

For most carcinomas, progression to malignancy is accompanied by a loss of epithelial differentiation and a shift toward a mesenchymal phenotype, *i.e.*, epithelial to mesenchymal transition (EMT).[7] EMT increases migration and invasiveness of many cell types and is often one of the conditions for tumor infiltration and metastasis. However, following invasion or metastasis, cells that have undergone the process of EMT can also revert to a well-differentiated epithelial phenotype.[8] In support of this, there exist numerous examples of advanced carcinomas showing that mesenchymal cells can regain characteristics of epithelial cells or undergo mesenchymal to epithelial transition (MET).[8–10] Both EMT and MET are regulated through an intricate interplay of RNA binding protein/miRNA complexes, including LIN28/miR-let7 and miR-200/ZEB.[9,10]

Intratumoral drug penetration and resistance

Potential causes of drug resistance in solid tumors include genetically and epigenetically determined factors expressed in individual cells and those related to the solid tumor environment. The latter include tumor stroma cells and proteins that form a dense matrix as well as intercellular junctions that seal the space between tumor cells.[11] To be effective, drugs have to diffuse throughout the tumor to achieve a lethal concentration in all of the tumor cells. However, most drugs, in particular those based on nanoparticles or liposomes with diameters around 100 nm, do not diffuse more than a few cell layers from blood vessels implying that more distant tumor cells receive only subtherapeutic drug exposure.[11–13] Furthermore, several studies have shown that the upregulation of epithelial junction proteins correlates with increased resistance to therapy, including therapy with the two major classes of cancer drugs—monoclonal antibodies and chemotherapeutics.[14–16] We therefore hypothesized that transient opening of junctions would increase the therapeutic efficacy of, and potentially, overcome resistance to chemotherapy in advanced stage epithelial cancers.

[1]Division of Medical Genetics, University of Washington, Seattle, Washington, USA; [2]Washington National Primate Research Center, Seattle, Washington, USA; [3]Fred Hutchinson Cancer Research Center, Seattle, Washington, USA; [4]Academia Sinica, Taipei, Taiwan; [5]European Synchrotron Radiation Facility, Grenoble, France; [6]Compliment Corp., Seattle, Washington, USA; [7]Unit of Virus Host Cell Interactions, UMI3265, CNRS/EMBL/UJF, Grenoble, France; [8]Department of Pathology, University of Washington, Seattle, Washington, USA
Correspondence: A Lieber (lieber00@u.washington.edu)
Received 1 December 2014; accepted 20 January 2015

Adenovirus serotype 3-derived junction opener (JO-1)

We have recently reported that a group of human adenoviruses uses DSG2 as a receptor for infection.[17] Among the DSG2-targeting viruses is human adenovirus type 3 (HAdV3). HAdV3 is able to efficiently breach the epithelial barrier in the airway tract and infect airway epithelial cells. This is achieved by the binding of HAdV3 to DSG2 and subsequent intracellular signaling that results in transient opening of tight junctions between epithelial cells.[17,18] We have capitalized on this mechanism and generated a recombinant protein that contains the minimal structural domains from HAdV3 that are required to open the intercellular junctions in epithelial tumors. This protein is called "junction opener 1" (JO-1).[6,19–21] JO-1 is a small recombinant protein derived from the HAdV3 fiber.[21] It contains two self-dimerizing trimeric HAdV3 fiber knob. JO-1 can be easily produced in *Escherichia coli* and purified by affinity chromatography. Binding of JO-1 to DSG2 triggers shedding of the DSG2 extracellular domain and activation of pathways that are reminiscent of an epithelial to mesenchymal transition (EMT), including the phosphorylation of MAP kinases and the downregulation of junction proteins.[17,19,20] Both mechanisms result in transient opening of epithelial junctions. Importantly, multimerization of the trimeric HAdV3 fiber knob through a K-coil motif is required for DSG2-triggered signaling and junction opening.[21]

Furthermore, we have recently shown that during HAdV3 replication, viral protein complexes, so called penton-dodecahedra (PtDd), that are structurally similar to JO-1, are released from infected cells, open the junctions between neighboring cells and thus allow *de novo* produced virus to spread in epithelial tumors.[18] A similar positive feed-forward mechanism should work for JO-1 penetration in tumors. We have shown in over 25 xenograft models that the intravenous injection of JO-1 increased the efficacy of cancer therapies, including monoclonal antibodies and chemotherapy drugs, in a broad range of epithelial tumors.[6,19] Further studies have shown that the effective doses of chemotherapy drugs can be reduced when they are combined with JO-1.[6]

The homology between the human and mouse DSG2 gene is 77.1% and neither HAdV3 nor JO-1 binds to mouse cells.[20] We therefore generated transgenic mice that contain the 90 kb human DSG2 locus including all regulatory regions. These mice express human DSG2 in a pattern and at a level similar to humans.[20] Furthermore, we have shown that JO-1 triggers hDSG2-mediated signaling and opening of epithelial junctions in epithelial mouse tumor cells that ectopically express hDSG2.[20] This indicates that human DSG2 can interact with mouse cytoskeletal proteins and kinases and implies that hDSG2 transgenic mice can be used as a model to study downstream effects of JO-1 binding to DSG2 after intravenous injection. The intravenous injection of JO-1 into hDSG2 transgenic mice was safe and well-tolerated.[17,19] Using hDSG2 transgenic mice, we also demonstrated that JO-1 predominantly acts on junctions in tumors.[6] A number of factors could account for this finding, including: (i) overexpression of hDSG2 by tumor cells, (ii) better accessibility of hDSG2 on tumor cells, due to a lack of strict cell polarization compared to hDSG2-expressing normal epithelial cells, and (iii) a high degree of vascularization and vascular permeabilty in tumors. Because of its preferential binding to and action on epithelial junctions of tumors, JO-1 appears to create a "sink" for therapeutic drugs in tumors, which decreases the levels and exposure of these drugs in normal tissues, at least in mouse tumor models (with a tumor weight to body weight ratio of 1:20).[20] This "sink" effect will most likely be less pronounced in cancer patients. Furthermore, we have shown in hDSG2 transgenic mice with syngeneic tumors that JO-1 remains active in the presence of anti-JO-1 antibodies generated by JO-1 vaccination of mice.[6,22] This may be due to the fact that JO-1 binds to DSG2 with a very high avidity thus disrupting potential complexes between JO-1 and anti-JO1 antibodies.

Clinical trial with affinity-enhanced junction opener (JO-4)

More recently, by screening of a mutant HAdV3 fiber knob library, we identified a series of (trimeric) HAdV3 fiber knob mutants with increased affinity to DSG2.[22] The highest affinity was conveyed by a specific mutation of valine residue at position 239 to an aspartatyl residue (V239D). Preliminary data showed that the dimerized form of this mutant (called JO-4) was therapeutically more potent than JO-1 in a series of cancer models.[22] Our goal is to use JO-4 in combination with Doxil, a PEGylated, liposome-encapsulated form of doxorubicin, in ovarian cancer patients. Doxil is FDA approved for treatment of advanced ovarian cancer patients that failed first line platinum therapy and is a preferred agent in this setting. When used as a monotherapy, objective response rates from 10 to 26% have been reported.[23–25] At the FDA recommend dose of 50 mg/m^2, monotherapy with Doxil is associated with grade 3 or worse toxicity in 30% of patients with hand-foot syndrome and stomatitis/mucositis being the most common. Doses have to be reduced to as low as 30 mg/m^2 in combination regimens which may be limiting efficacy.

In this study, we provide preclinical data showing in an ovarian cancer mouse model that the combination with JO-4 allows salvaging the therapeutic effect of Doxil when given at a dose threefold lower than the therapeutic dose. Furthermore, we provide preclinical data in a xenograft model that JO-4 also increases the therapeutic effect of Doxil on lymphogenic metastases. In preparation of an Investigational New Drug (IND) application, we have performed a toxicity and biodistribution study of combined JO-4 and Doxil treatment in *Macaca fascicularis*. This study showed that the combination therapy is safe in an adequate animal model.

RESULTS

Structural and functional characterization of JO-4

JO-4 is a dimeric form of the trimeric HAdV3 fiber knob with each fiber knob monomer containing a V→D substitution in amino acid position 239. Valine is a small hydrophobic amino acid residue while aspartic acid is negatively charged. The mutation is localized in the EF loop of each HAdV3 knob monomer (Figure 1a). X-ray crystallography of the nondimerized, trimeric HAdV3-V239D fiber knob showed that the EF loop in V239D is displaced with respect to the wild type due to the formation of a salt bridge between Asp239 and Lys275 (Figure 1b,c). The Lys275 side chain rotamer adopts a different conformation in the V239D mutant compared to wild type in order to interact with Asp239. This salt bridge locks the EF loop into a new conformation, potentially explaining the increased binding affinity for the receptor. Detailed data on the analysis of HAdV3 knob V239D crystals are shown in Table 1. We previously demonstrated that the affinity of the HAdV3-V239D fiber knob (K_D = 11.4 nmol/l) is 885-fold higher than the parental, nonmutated fiber knob (K_D = 10.1 µmol/l).[22]

Here we studied the interaction of the self-dimerizing HAdV3-V239D fiber knob, *i.e.*, JO-4, with DSG2 by surface plasmon resonance analysis (Figure 1d). The DSG2 interaction to mobilized JO-4 had a high affinity with a K_D in the nanomolar range (K_D = 1.4 nmol/l). This high affinity can be explained by both a high association rate ($k_a = 3.3 \times 10^5$ M^{-1}s^{-1}) and, by the very slow dissociation ($k_d = 4.7 \times 10^{-4}$ s^{-1}). This feature is clearly seen in the sensorgrams

at the end of the injection where the signal remains stabile for the time of analysis.

In summary of our structural studies, we concluded that the new conformation of the EF loop in JO-4 potentially explains its high affinity to DSG2.

JO-4 co-therapy allows for reduction of effective Doxil dose in a xenograft model of ovarian cancer

In the majority of cancer patients, the dose of Doxil has to be reduced from 50 mg/m^2 to less than 30 mg/m^2 due to toxicity. One of our clinical objectives is to test whether JO-4 can salvage the therapeutic effect of a lower dose of Doxil. We performed a study in mice with xenograft tumors derived from primary ovarian cancer ovc316 cells. Ovc316 cells were obtained from a patient and closely model the heterogeneity and plasticity seen in tumors *in situ*.[26] Mice with pre-established, mammary fat pad-localized ovc316 tumors were weekly intravenously injected with JO-4 at a dose of 2 mg/kg, followed 1 hour later by an intravenous injection of Doxil at a therapeutic dose of 3 mg/kg or a subtherapeutic "low" dose of 1 mg/kg (Figure 2a). This study shows higher antitumor efficacy of JO-4 plus "low"-dose Doxil (1 mg/kg), compared to "high" dose Doxil alone (3 mg/kg), indicating that it is possible to lower the effective dose of Doxil when combined with JO-4.

JO-4 increases the therapeutic effect of Doxil on lymphogenic metastases

As outlined above, in order to metastasize, epithelial cancer cells acquire mesenchymal features through EMT. There is strong support that, once metastatic cells homed to other tissues, they regain epithelial features, including epithelial junctions.[9,10] To corroborate this, we employed a model of epithelial breast cancer that forms spontaneous metastases. The model is based on MDA-MB-231-luc-D3H2LN cells which allow for *in vivo* imaging of tumor growth based on luciferase expression. Tumor cells injected into the mammary fat pad formed axillary lymph node metastases if the primary tumor was removed 5 weeks after inoculation (Supplementary Figure S1a). If the primary tumor is not removed, it invades the peritoneum (Supplementary Figure S1b) and forms metastases in mesenteric lymph nodes that are clearly distinguishable from the primary tumor by *in vivo* imaging (Figure 2b). Immunofluorescence analysis of tumor sections showed signals consistent with membrane localization of DSG2 in the primary tumor and metastatic lesions (Figure 2c, Supplementary Figure S1b). The amount of DSG2, as assessed by western blot analysis, was comparable in the primary and secondary tumors (Figure 2d). To address the question whether JO-4 can also act on metastases, we performed a therapy study in the model with invasive tumors that form lymphogenic metastases in mesenteric lymph nodes. Treatment (phosphate-buffered saline (PBS), Doxil (1 mg/kg) alone, JO-4 (2 mg/kg) + Doxil) was started when metastases were clearly detectable by *in vivo* luciferase imaging. Luminescence signals for the primary and secondary lesions were recorded separately the day before treatment and at day 5 after treatment and expressed as a ratio to show tumor progression (Figure 2e,f, Supplementary Figure S2). In most untreated mice, both primary tumor and metastases grew. Regression of the metastatic lesions was observed in one out of five Doxil-treated mice. Tumors in the remaining four animals did not respond to Doxil. In contrast, all primary tumors and three out four metastatic lesions shrank when mice were treated with the combination of JO-4 and Doxil. This suggests that in this model, JO-4 can enhance the therapeutic efficacy of Doxil against metastases.

JO-4 injection is safe in human DSG2 transgenic mice

There were no adverse effects or critical abnormalities in hematologic and serum chemistry parameters or histopathological studies

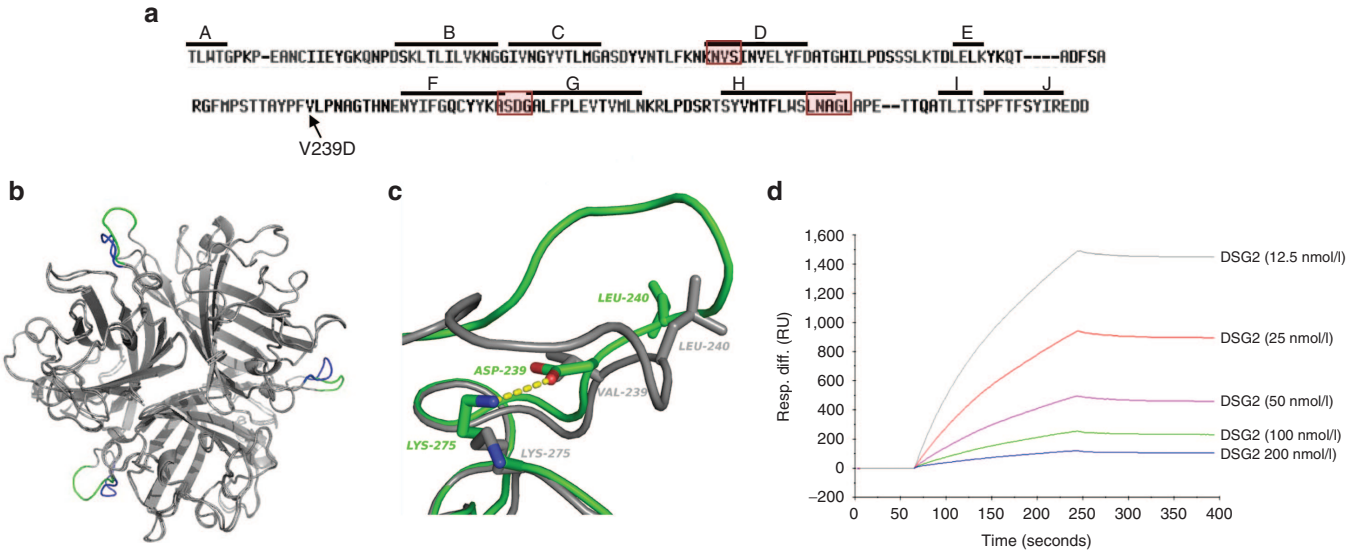

Figure 1 Structural and functional studies with JO-4. (**a**) HAdV3 fiber knob amino acid sequence with β sheets A to J indicated by a line. JO-4 contains HAdV3 fiber knobs with a valine to aspartic acid substitution in position 239 of the HAdV3 fiber knob. Regions that have previously been found to be involved in DSG2 binding are boxed.[22] (**b**) 3D-structure superimposition of the trimeric (wild type) HAdV3 fiber knob and the V239D mutated fiber knob. The common structure appears in grey, the EF loops of wild-type and mutant HAdV3 knob monomers are labeled in blue and green, respectively. (**c**) Shown is the interactions between D239 and K275 in the mutant and the new position of the L240 residue. Residue labels are colored green for the mutant and gray for wt. H-bonds between D239 and K275 are shown in dashes. (**d**) Affinity of JO-4 to DSG2 measured by surface plasmon resonance. JO-4 was immobilized on sensorchips, and background was automatically subtracted from the control flow cell. DSG2 were injected for 3 minutes at a concentration range from 12.5 to 200 nmol/l and kinetics and affinity parameters were evaluated using the BIAeval software ($k_a = 3.3 \times 10^5$ M^{-1}s^{-1}; $k_d = 4.7 \times 10^{-4}$ s^{-1}; K_D =1.4 nmol/l).

of tissues after intravenous injection of JO-4 (2 and 10 mg/kg) into hDSG2 transgenic mice with or without pre-existing anti JO-4 antibodies (data not shown). After injection of 10 mg/kg, we observed a mild lymphocytopenia and intestinal inflammation that subsided by day 3 after injection.

Intravenous JO-4 injection into nonhuman primates (NHP) is safe (NHP study #1)

HAdV3 and HAdV3 fiber knobs do not efficiently bind to mouse,[20] rat, hamster, and dog PBMCs or transformed cell lines (data not shown) and the DSG2 gene homology for these species compared to human DSG2 is less than 80%. Although hDSG2 transgenic mice allow us to study a number of variables in a large number of animals, it is unclear whether the hDSG2-mouse system accurately models a homologous system with human DSG2 in human cells. Better models are NHPs. The DSG2 gene homology between humans and macaques is 96.6%. We have shown that the DSG2 expression pattern and level in tissues of *M. fascicularis* is similar to humans.[20] HAdV3 and HAdV3 derivatives bind to monkey DSG2 and trigger junction opening at a level that is comparable to human cells.[20] This justifies the use of *M. fascicularis* for toxicology studies in preparation of an IND package. A preliminary study was conducted in which two animals (~5 kg) were injected intravenously with a single dose of JO-4 (0.6 mg/kg) (Figure 3a). This dose was chosen because, after allometric scaling, it corresponded to 2 mg/kg of JO-4 used in mice (http://www.fda.gov/downloads/Drugs/Guidances/UCM078932.pdf). The animals were monitored by an independent group of veterinarians and pathologists at the Washington State Northwest Primate Research Center at the University of Washington. Blood samples were taken daily. A full necropsy was performed at day 3 after JO-4 injection (see Supplementary Materials: "NHP study #1). There was no evidence of changes in health/behavior, laboratory studies or pathologies. Histological analysis revealed a mild gastro-enterocolitis, which is often observed in monkeys in this center. Analysis of hematological parameters revealed a mild lymphopenia at day 1, thrombocytopenia at days 1, 2, and 3 (Figure 3b). A mild transaminitis was observed at day 1 after JO-4 injection which could be related to residual bacterial endotoxin (20 EU/mg) in the JO-4 preparation. This is supported by elevated serum γ–interferon levels observed within hours after JO-4 injection (Figure 3b), a response that can be attributed by lipopolysaccharide endotoxin (LPS) activation of tissues macrophages. We are currently working on the clinical grade production of JO-4 which will also remove all LPS from the preparation.

Combined treatment with JO-4 and Doxil is safe in NHPs (NHP study #2)

A second study in male *M. fascicularis* was performed to address the question whether JO-4 increases Doxil toxicity. One animal (A-88) was injected intravenously with JO-4 at a dose of 2 mg/kg*, *i.e.*, at a dose that was effective in mouse models. (In a pre-IND meeting initiated after NHP study#1, the FDA recommended not to use allometric scaling for NHP dose selection in macaques.) Another animal (A-93) was injected with saline. One hour later, both animals received an intravenous injection of Doxil at a dose of 40 mg/m^2 (1.1 mg/kg), *i.e.*, at a dose that will be used in the clinical trial (Figure 4a). Animals were monitored daily and blood samples were collected at 4, 6, and 24 hours and then at day 3, 7, and 14 after Doxil injection. At day 14, animals received a second cycle of treatment. At 6 hours after the second Doxil injection, animals were euthanized and a gross necropsy was performed by a certified veterinary pathologist. The rationales for the second injection cycle followed by the necropsy were (i) to assess potential anaphylactic reactions in a treated animal with serum antibodies against JO-4, (ii) to assess JO-4 tissue distribution, and (iii) to study the effect of JO-4 on Doxil serum clearance and tissue uptake.

Table 1 Collection and refinement statistics

Data collection	
Space group	P41212
Cell dimensions	
a, *b*, *c* (Å)	137.6, 137.6, 108.9
α, β, γ(°)	90, 90, 90
Resolution (Å)	44–2.65 (2.74–2.65)[a]
R_{sym} or R_{merge}	0.105 (1.43)
$I/\sigma I$	18.9 (1.43)
Completeness (%)	99.0 (90.3)
Redundancy	8.9 (8.6)
Refinement	
Resolution (Å)	44–2.65 (2.74–2.65)
Number of reflections	30,618 (2,704)
R_{work} or R_{free}	0.176/0.205
Number of atoms	
Protein	4,442
Ligand/ion	295
Water	245
B-factor	
Protein	70.
Ligand/ion	135.
Water	70.
R.m.s deviations	
Bond length (Å)	0.01
Bond angles (°)	1.17

[a]Highest resolution shell is shown in parentheses.

Vital symptoms. Daily monitoring showed no abnormal changes in body weight, food intake, infusion site appearance, body temperature, posture, respiration, feces/urine, food water, recumbent, attitude, and skin (data not shown). ECGs, taken before treatment and 24 hours, 3, 7, and 14 days after the first injection cycle and 6 hours after the second injection cycle, were normal (data not shown).

Pathology and histology after necropsy. At necropsy, animals were in good health; no external lesions were observed and all body systems and organs appeared grossly unremarkable. Histology analysis of sections from 39 tissues showed mild gastroenterocolitis in both animals, a condition that is commonly seen in the colony and not related to the treatment. Histology of all other tissues was normal or interpreted as nonspecific background or incidental findings. Bone marrow cytology was unremarkable. The full pathology report can be found in the Supplementary Materials: "NHP study #2.

Blood cell counts and chemistry. CBC analysis showed mild leukocytosis starting at day 7 after treatment in both animals due to an increase in neutrophiles (Figure 4b). In addition, animal A-88 also showed increased lymphocyte counts at day 3 and 7 after the first treatment cycle and 6 hours after the second treatment that was most likely related to JO-4 injection. A mild lymphocytopenia was seen at day 14 after the first treatment most likely due to Doxil treatment. A transient elevation of serum aspartate aminotransferase (AST) after the treatment was observed in both animals. In the JO-4-treated animal, transiently increased serum alanine aminotransferase (ALT/SGPT) levels were detected at 24 hours after injection (Figure 4c). JO-4 injection also increased the serum levels of IFN-γ up to day 3 after injection (Figure 4d). Considering studies in mice, the transient elevation of IFN-γ and ALT could be due to residual amounts of bacterial LPS in the JO-4 preparation (2.2 EU/mg). Because in studies with mouse tumor models, JO-1 caused cleavage of the extracellular domain (ECD) of DSG2, we measured the concentration of soluble DSG2 ECD in serum (Figure 4e). While clearly detectable, no JO-4-related effects on the kinetics of serum DSG2 concentration were observed.

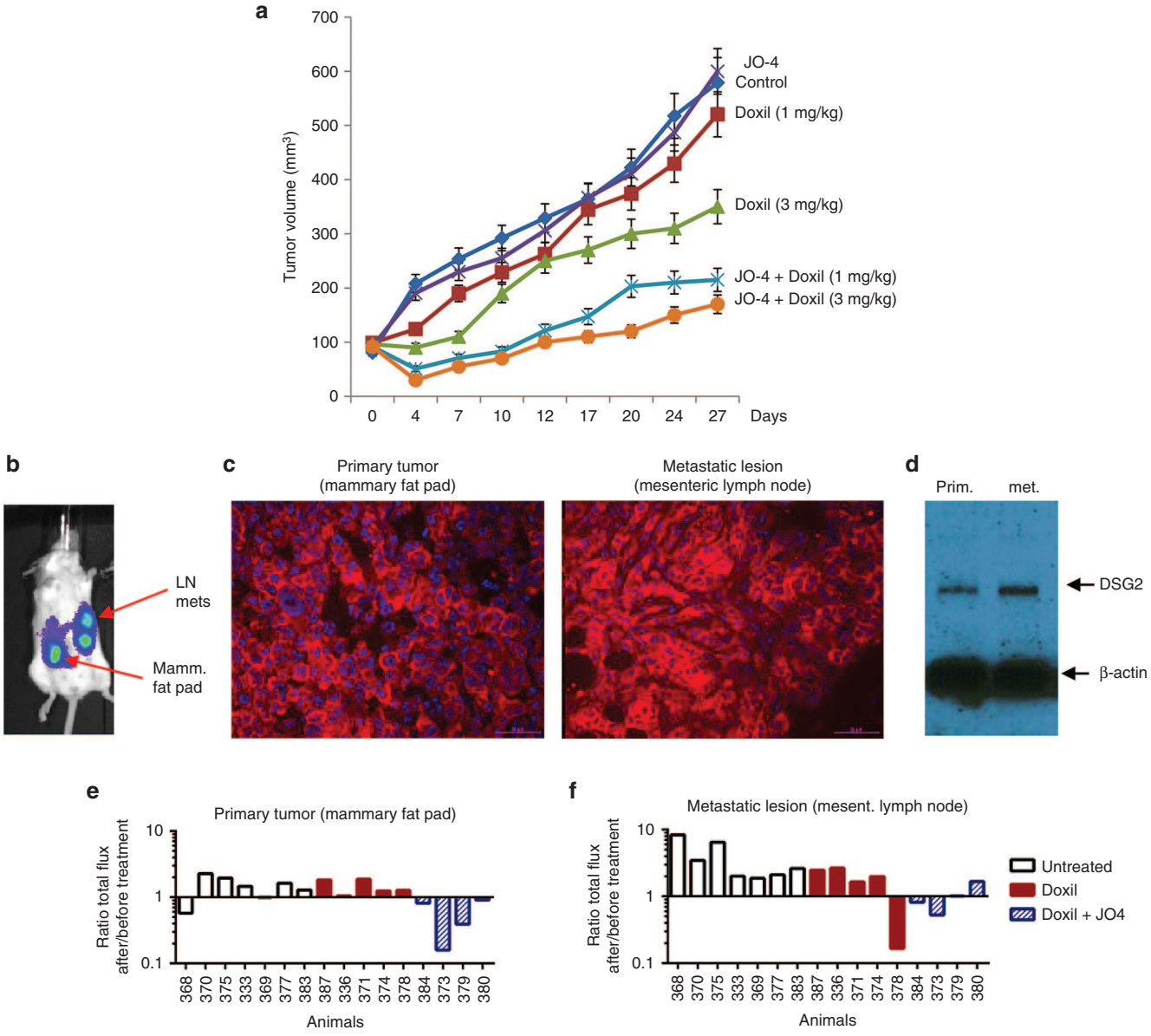

Figure 2 Efficacy studies with JO-4 and Doxil in mouse models. (**a**) Efficacy study in mammary fat tumor pad model using primary ovarian cancer (ovc316) cells. Treatment was started when tumors reached a volume of 100 mm^3. Mice were injected intravenously with Doxil (1 or 3 mg/kg) alone or in combination with 2 mg/kg JO-4. Treatment was repeated weekly. $N = 10$. (**b–f**) Studies in the spontaneous metastasis model based on MDA-MB-231-luc-D3H2LN cells. (**b**) *In vivo* luciferase imaging of a representative animal. The primary tumor in the mammary fat pad forms metastasis in regional lymph nodes (LN), *e.g.*, pancreatic and mesenteric lymph nodes. (**c**) DSG2 immunofluorescence analysis of sections from the primary tumor and mesenteric lymph node metastases. DSG2 signals are in red and appear to be membrane associated. Nuclei are stained in blue. (**d**) Western blot analysis of primary tumor and metastases with DSG2 antibodies. β-actin is used as a loading control. A representative animal is shown. (**e,f**) Comparison of *in vivo* luciferase signal in the primary tumor (**e**) and metastasis (**f**) 1 day before and 5 days after treatment with Doxil or JO-4 + Doxil. Shown is the total flux of the primary tumor or metastasis ROI after treatment divided by the ROI before treatment. Shown are averages of imaging sequences of five images each. The difference between the Doxil and Doxil+JO4 groups is significant ($P < 0.01$) for both the primary tumor and the metastases. The difference between the untreated and Doxil groups is not significant.

Serum and tissue samples were used to measure JO-4 and Doxil concentrations as well as antibodies against JO-4.

JO-4 serum clearance and biodistribution. In the JO-4-injected animal A-88, serum JO-4 levels declined to undetectable levels by day 3 after injection (Figure 5a). A second injection resulted in similar levels at 4 hours after injection and similar decline by 6 hours. IgG antibodies specific to JO-4 became detectable in serum at day 7 and increased by day 14 (Figure 5b). After the second JO-4 injection, anti-JO-4 IgG dropped to background levels. This indicates that a fraction of the injected JO-4 forms complexes with anti-JO-4 antibodies which are then either taken up by tissues or are not detectable by enzyme-linked immunosorbent assay (ELISA) due to epitope masking. Further studies with tissue samples support the first scenario (see below). JO-4 concentrations and levels of anti-JO-4 antibodies in tissue lysates were measured by ELISA (Figure 5c,d). When considered together, the data suggest the following: In animal A-88, JO-4 was present in epithelial tissues such as the adrenal glands, epididymis, gall bladder, kidneys, lung, and pancreas (Figure 5c). Immunofluorescence staining of the adrenals, epididymis, kidney, and lungs against JO-4 showed association of signals with the membrane of epithelial cells in animal A-88 (Figure 6a,b). Together with JO-4, anti-JO-4 antibodies were found in a series of organs including adrenals, epididymes, eye, lungs, colon, cecum, lymph nodes, prostate, spleen, stomach, and urinary bladder suggesting opsonization of antibody-JO-4 complexes. The latter is supported by immunofluorescence studies that showed colocalization of a fraction of JO-4 with IgG. (Figure 6c). In the liver, JO-4 was predominantly found in association with Kupffer cells (Figure 6d). The finding that JO-4 strongly localized to adrenals was unexpected. The adrenal glands are one of the organs that have the greatest blood supply per gram of tissue and the JO-4 and JO-4 immune complex signals in this tissue might, in part, originate from residual blood.

Doxil serum clearance and biodistribution. Doxil concentrations were measured by ELISA using two monoclonal antibodies that recognize PEG in nanoparticles.[27] Serum clearance of Doxil after intravenous injection (Figure 7a) is consistent with the expected half-life of ~80 hours in humans.[28] There was a slower decrease of serum Doxil concentrations during the first 24 hours in the animal that received JO-4 (A-88). Doxil was undetectable in both animals at day 14. A second injection resulted in higher Doxil concentrations at 4 and 6 hours in animal A-88. Doxil concentrations were also measured by ELISA in tissues samples (Figure 7b). The highest Doxil concentrations in animal A-93 (w/o JO-4) were found in adrenals, bone marrow, brain, heart, GI tract, liver, mesenteric lymph nodes, seminal vesicle, and spleen. JO-4 injection (animal

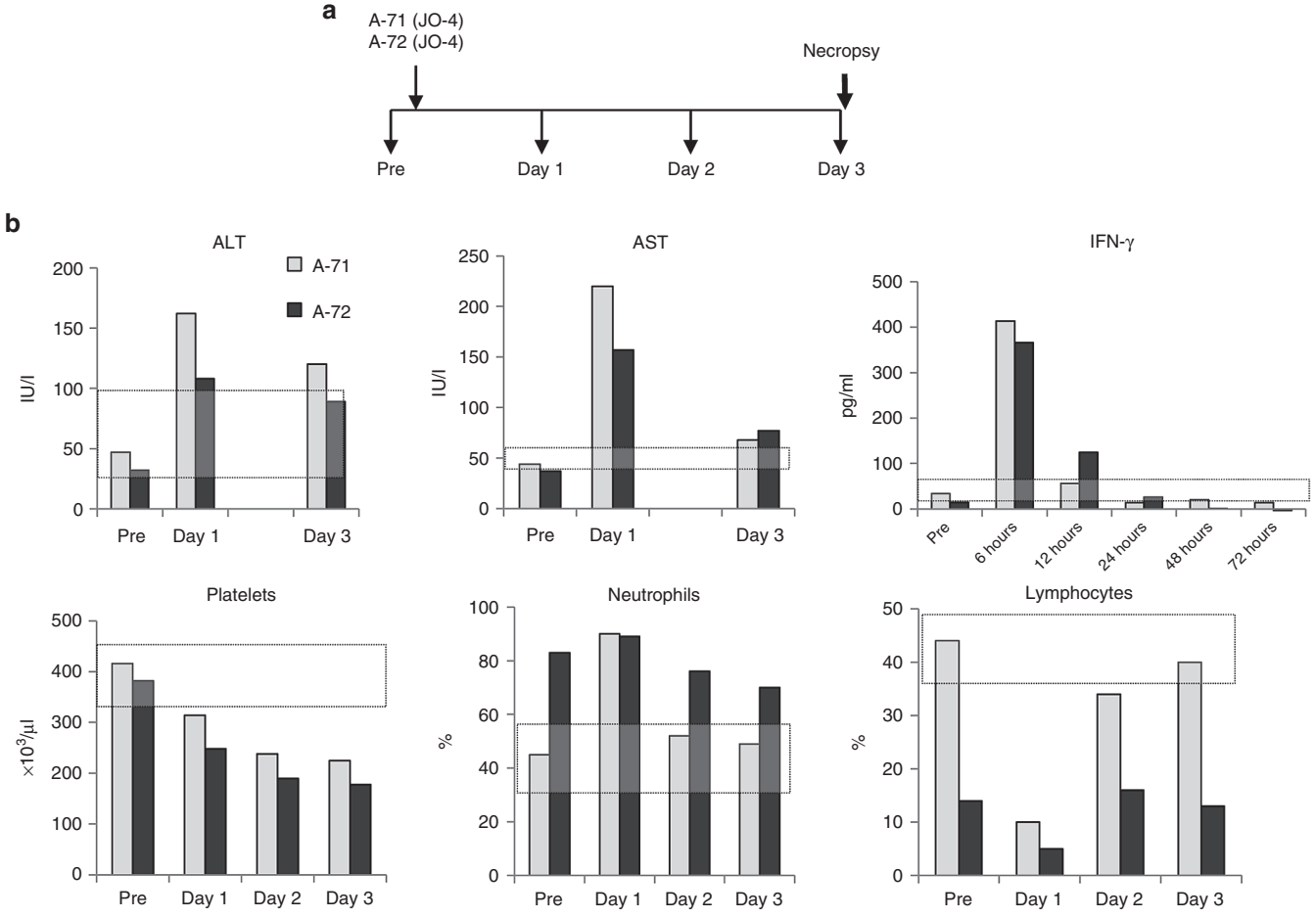

Figure 3 Nonhuman primates (NHP) study #1 (JO-4 alone): Three day toxicity study in macaques injected intravenously with 0.6 mg/kg of JO-4. (**a**) Experimental design. Two sedated *M. fascicularis*, A10271 (A-71) (age: 4 years 8 months, weight 5.5 kg) and A10272 (A-72) (age: 5 years, weight: 6.96 kg) were injected through the saphenous vein with 5 ml of JO-4 at a dose of 0.6 mg/kg at an infusion rate of 2 ml/minute). Blood samples were collected daily. A full necropsy was performed at day 3. (**b**) Shown are hematological parameters that were different from normal. The normal range is marked by the gray-shaded area.

A-88) resulted in increased Doxil accumulation in the epididymes and the liver. Interestingly, Doxil concentrations in A-88 were lower in the adrenals, bone marrow, heart, lymph nodes, seminal vesicle, and spleen compared to the animal that did not receive JO-4. We speculate that JO-4 increases the liver's capacity to trap Doxil so that other tissues are less exposed. Notably, transaminases were slightly higher in the JO-4-treated animal (Figure 4c). Immunofluorescence studies on sections from adrenals and kidneys were in agreement with the Doxil ELISA data (Figure 6e).

In summary, analysis of vital symptoms, blood parameters, and organ histology did not show remarkable signs of toxicity. Upon necropsy, no significant treatment-related abnormalities in gross examination of organs and histological analysis of tissue sections were observed. Although JO-4 accumulation was found in normal tissues, this did not appear to cause toxic effects. We therefore concluded that the combination of JO-4 and Doxil was well tolerated in a NHP model.

DISCUSSION

Malignant cells in epithelial ovarian cancer are linked through junctions, which inhibit drug penetration into the tumor implying that cancer cells that are farther away from blood vessels receive only subtoxic concentrations of drugs and are not affected by chemotherapy or become prone to develop resistance.[29,30] Epithelial junctions in particular are a barrier for tumor penetration of newer generations of chemotherapy drugs based on liposomes or

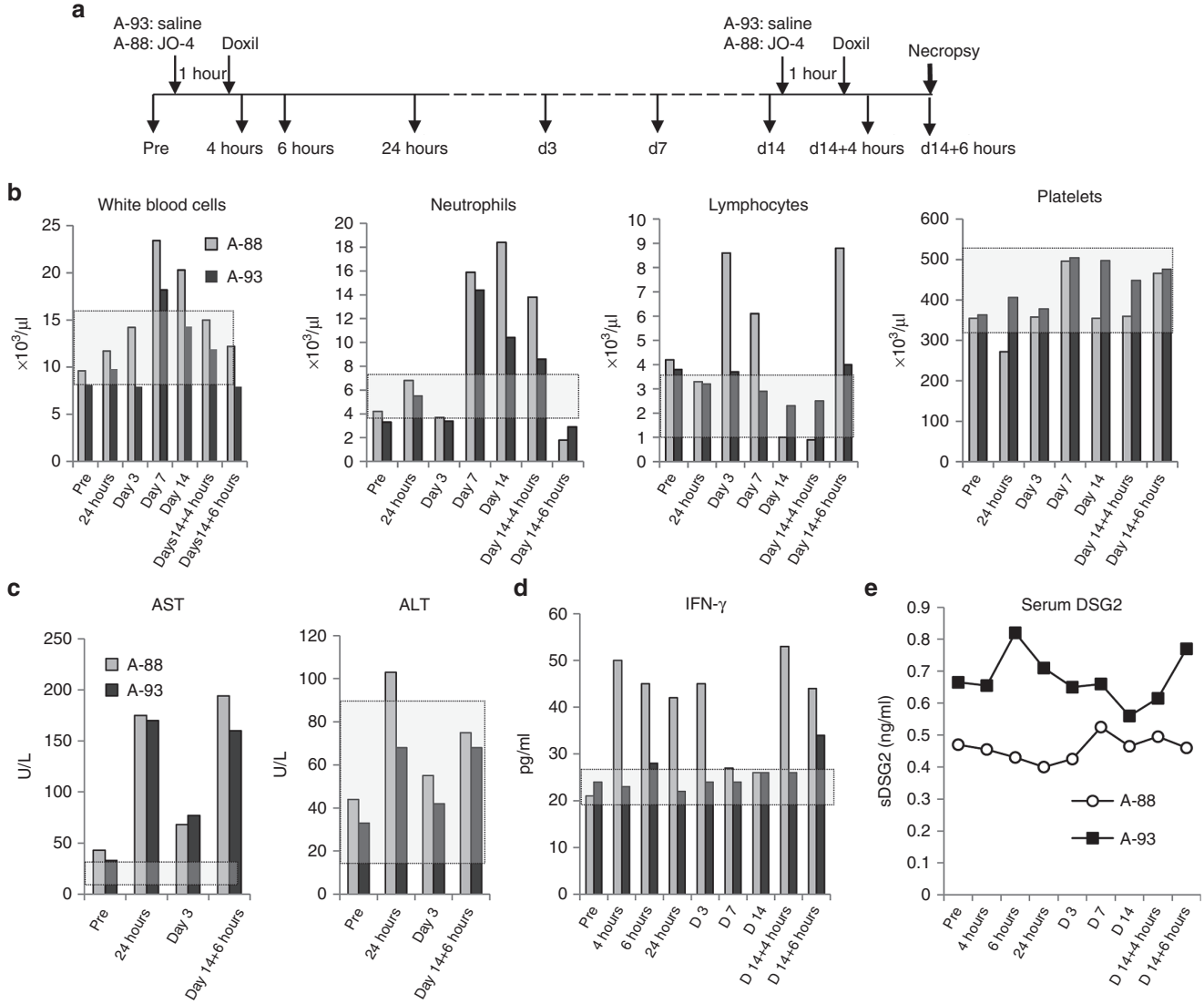

Figure 4 Nonhuman primates (NHP) study #2 (JO-4+Doxil): Blood analysis. (**a**) Experimental design: Two sedated *M. fascicularis*, A11288 (A-88) (age: 4 years 11 months, weight: 5.0 kg) and A11293 (A-93) (age: 5 years 10 months, weight: 6.1 kg) were injected through the saphenous vein with 5 ml of saline (A-93) or 5 ml of JO-4 at a dose of 2 mg/kg (A-88) at an infusion rate of 2 ml/minute). One hour later, both animals received an intravenous injection of 20 ml of Doxil at a dose of 40 mg/m^2 (1.1 mg/kg). Blood was collected at the indicated time points. (**b**) One set of blood samples was submitted to the UW Clinical Laboratory for CBC and blood chemistry analysis. A second set of plasma samples was used for measuring the concentrations of JO-4, anti-JO-4 antibodies, Doxil, DSG2, and proinflammatory cytokines. Blood cell counts: Treatment-related changes were observed for white blood cells, neutrophiles, and lymphocytes. All other hematological parameters including red blood cell, platelet, monocyte, eosinophil, basophil counts were normal. (**c**) Blood chemistry: Treatment-related changes were observed for AST and ALT. Sodium, potassium, chloride, glucose, blood urea nitrogen, creatinine, total protein, albumin, globulin, A:G ratio, total bilirubin, calcium, magnesium, phosphate, cholesterol, alkaline phosphatase, and GGT levels were unremarkable. (**d**) Serum interferon-γ levels were measured by ELISA. For all analyzed serum proteins, at least two serum dilutions in duplicates were analyzed in two independent ELISAs. (**e**) Serum DSG2 (sDSG2) ECD concentrations.

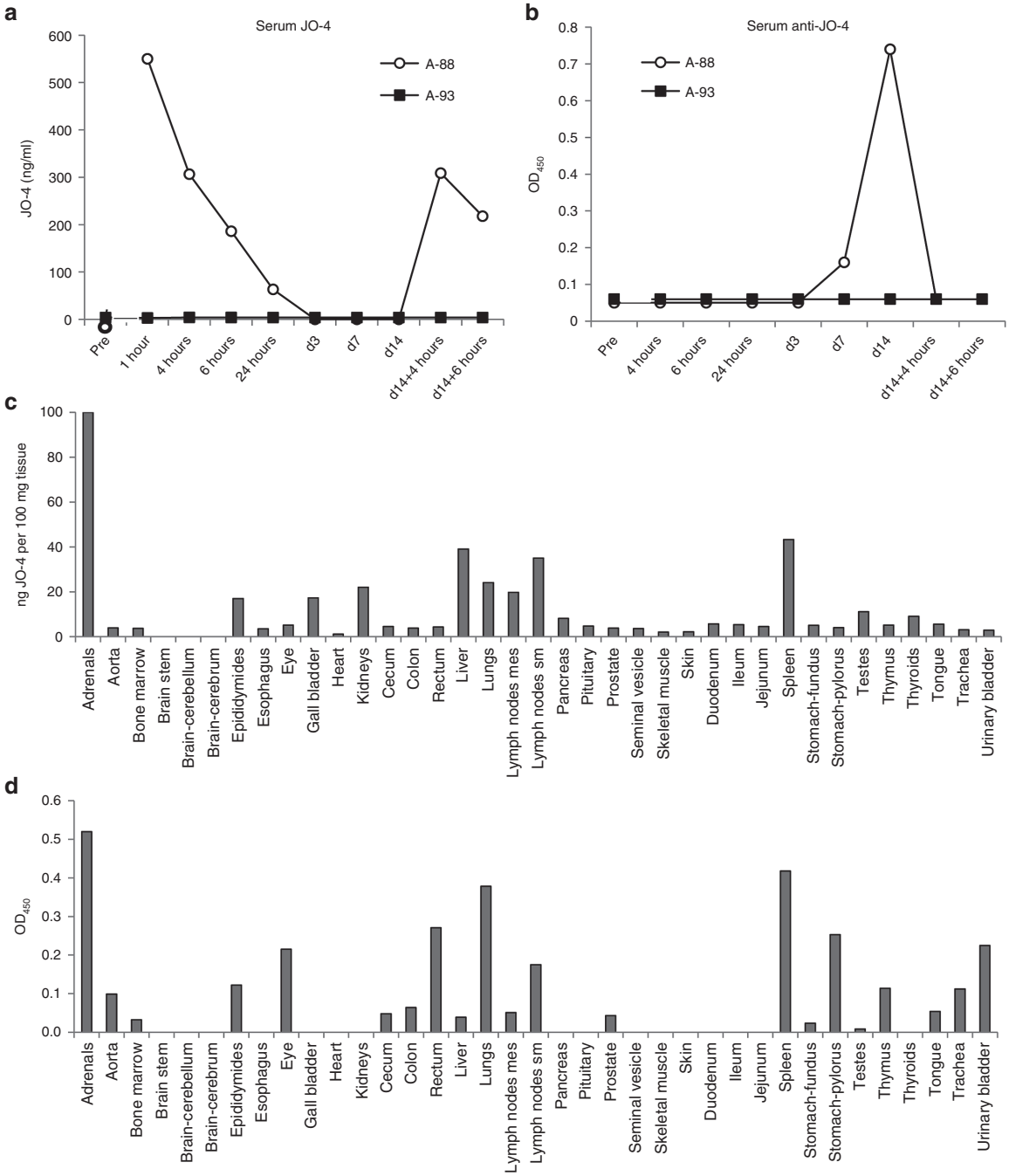

Figure 5 Nonhuman primates (NHP) study #2 (JO-4+Doxil): JO-4 analysis. (**a**) JO-4 concentrations were measured by enzyme-linked immunosorbent assay (ELISA). In animal A-88, there was no JO-4 detectable before injection. Animal A-93 did not show detectable JO-4 signals at all. (**b**) anti-JO-4 serum antibodies. Polyclonal HAdV3 fiber antibody was absorbed on ELISA plates followed by JO-4 protein at a saturating concentration. Dilutions of monkey serum (1:10, 1:100, and 1:1,000) were added and binding was detected with either goat-anti monkey IgG+IgA+IgM-HRP or goat anti-monkey IgG-HRP (MyBioSource). There were no significant differences in OD450 values for both conjugates indicating that most of the anti-JO-4 antibodies were IgG. Shown is OD450 at 1:100 dilution, using anti-monkey IgG conjugate. (**c**) JO-4 concentrations in tissues. (**d**) anti-JO-4 antibodies (OD450 per 100 mg/tissue).

nanoparticles which often have a diameter greater than 100 nm.[13] We have developed a recombinant protein (JO-1) capable of transiently opening epithelial junctions and increasing intratumoral chemotherapy drug accumulation and penetrations. Our goal is to test an affinity enhanced version of this junction opener (JO-4) in combination with Doxil in ovarian cancer patients. We therefore performed a series of preclinical safety and efficacy studies in support of an IND application.

JO-4 has a single amino acid mutation in the EF loop of the DSG2 interacting domain, the HAdV3 fiber knob. This V239D substitution changes the conformation of the EF loop as determined by X-ray crystallography. Interestingly, the L240 amino acid next to the V239D mutation has been previously reported as one of the putative critical residues for the receptor interaction.[31] In the crystal structure, the position of the backbone and side chain of Leu240 is altered with respect to the wild type. Leu240 is exposed to the

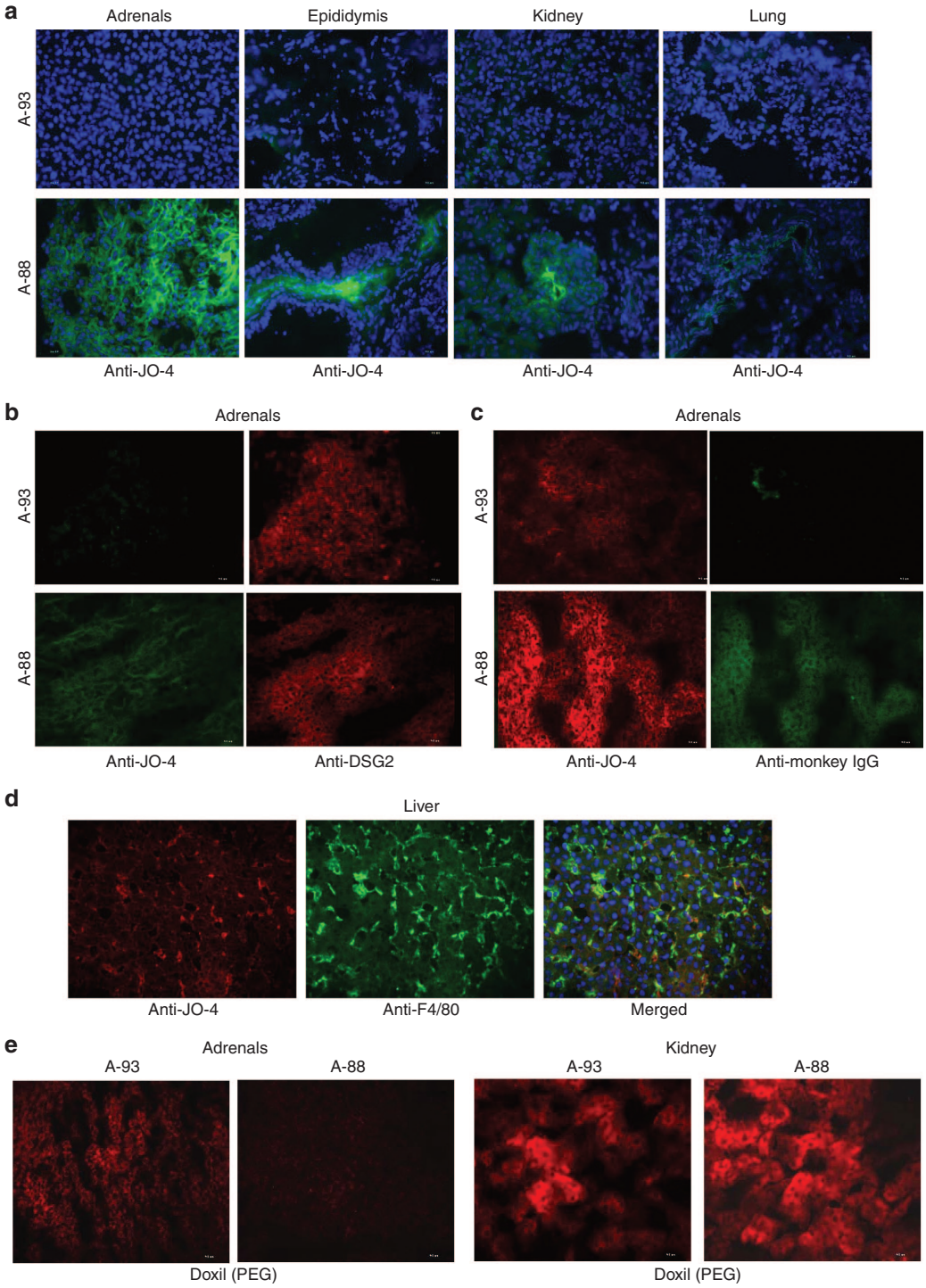

Figure 6 Nonhuman primates (NHP) study #2 (JO-4+Doxil): Immunofluorescence analysis of tissue sections. (**a**) Presence of JO-4 in tissues. Staining for JO-4 appears in green, nuclei are blue. (**b**) Staining of adrenals sections with anti JO4 antibodies (green) and anti-DSG2 antibodies (red). (**c**) Staining of adrenals section with anti JO-4 antibodies (red) and anti-monkey IgG-FITC from NIH Nonhuman Primate Reagent Resource (green). (**d**) Staining for JO-4 (red) and the Kupffer cell marker F4/80 (green). (**e**) Staining of adrenal and kidney sections for Doxil using antibodies against PEG (red).

solvent and the backbone of the EF loop is in a more extended conformation, possibly facilitating interactions with DSG2. Theoretically, this could bring the DSG2-interacting regions in the HAdV3 fiber knob (see Figure 1a,b) into closer proximity to DSG2, which, in turn could account for the higher affinity of the HAdV3-V239D fiber knob mutant compared to the wildtype HAdV3 fiber knob. To investigate these interactions in more detail, the atomic resolution of the HAdV3 fiber and V239D mutant in complex with the DSG2 ectodomain would be required.

An important finding in our studies with an ovarian cancer xenograft model was that JO-4 allowed Doxil to remain therapeutically active when applied at lower doses together with JO-4. This is clinically relevant because in almost all patients the Doxil doses have to be lowered due to toxicity that develops after several treatment

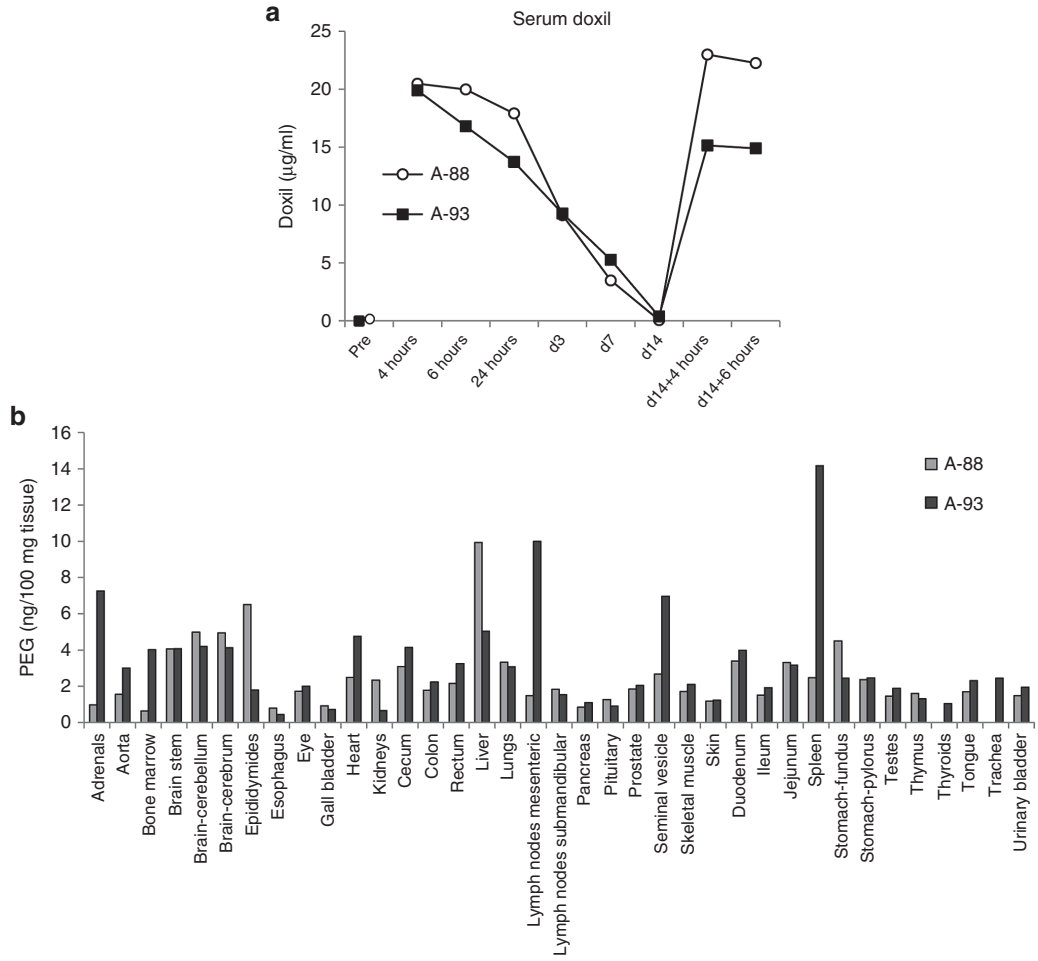

Figure 7 Nonhuman primates (NHP) study #2 (JO-4+Doxil): Analysis of Doxil concentrations measured by enzyme-linked immunosorbent assay. (**a**) serum Doxil levels. (**b**) Doxil concentration in tissues. Shown are average values from two independent samples of each organ.

cycles. While it is now acknowledged that, after metastasis, cancer cells regain an epithelial phenotype, including epithelial junctions, which protect cancer cells from immune attacks and treatment,[32] in the literature one can still find the misconception that metastatic lesions do not contain junctions, which would imply that JO-4 would not act on metastases. To address this, we employed a model of spontaneous metastasis. Immunofluorescene analysis of sections from metastases suggested membrane localization of DSG2. Efficacy studies in the metastasis model indicated the ability of JO-4 to promote reduction of the primary tumor and metastatic lesions by Doxil. These data with JO-4 in mouse models together with the preclinical efficacy data that we assembled for JO-1 give a solid basis that JO-4 has the potential to increase the therapeutic efficacy of Doxil in ovarian cancer patients.

A major concern was the safety of intravenously injected JO-4. The JO-4 target receptor DSG2 is expressed in most epithelial tissues. Our histology analyses however showed that DSG2 in normal epithelial tissues, which display a strict apical basal polarization, is trapped in lateral junctions and not readily accessible to intravenously injected ligands. In contrast, in epithelial tumors, this polarization is lost and DSG2 can be found on all membrane sides of tumor cells.[20] Safety of JO-4 is in part predicted by studies with HAdV3 or HAdV3 fiber knob containing vectors in humans. For more than a decade, Ad5 vectors that possess HAdV3 fibers (Ad5/3), which also infect cells through DSG2,[21] have been used for cancer therapy in animal models and humans with a very good safety profile after intravenous injection.[33,34] A recent phase 1 trial demonstrated safety of an intraperitoneally applied Ad5/3-based oncolytic vector in recurrent ovarian cancer patients.[35] Last year, we performed a study with an oncolytic vector based on HAdV3.[36] In this study, 25 patients with chemotherapy refractory cancer were treated intravenously with a fully serotype 3-based oncolytic adenovirus Ad3-hTERT-E1A. The only grade 3 adverse reactions observed were self-limiting cytopenias. Neutralizing antibodies against HAdV3 increased in all patients. Signs of possible efficacy were seen in 11/15 (73%) patients evaluated for tumor markers. Particularly promising results were seen in breast cancer patients and especially those receiving concomitant trastuzumab. The latter might suggest that HAdV3 acts in a similar way to JO-1 on tumor junctions and increases drug penetration.

We first confirmed that the intravenous injection of JO-4 was safe in hDSG2 transgenic mice. Next we tested JO-4 as a single agent in *M. fascicularis* at a relatively low dose (0.6 mg/kg) that we determined based on allometric scaling of the therapeutic dose used in mouse experiments. We followed the animals 3 days and performed a full necropsy to assess toxic side effects on normal tissues. In this study, we did not find critical JO-4-related abnormalities. In a second NHP study we combined JO-4 with Doxil. JO-4 was used at a dose that was effective in mouse tumor models (2 mg/kg). Doxil was injected at a dose that will be used in the clinical trial (40 mg/m^2). Analysis of clinical symptoms and blood parameters did not show

remarkable signs of toxicity. Upon necropsy, performed at 6 hours after the second injection cycle, no treatment-related abnormalities in gross examination of organs and histological analysis of tissue sections were observed. Therefore, the combination of JO-4 and Doxil was safe in an adequate animal model. Blood and tissue samples from the second study were also used to study JO-4 and Doxil blood clearance and tissue biodistribution. Despite the limitations of the study ($N = 1$), a series of cautious conclusions can be made: (i) The concentration of shed DSG2 in the serum did not increase after JO-4 injection, indicating minimal interaction with DSG2 on normal tissues. In contrast, in mouse tumor models, JO-4 triggered the cleavage and shedding of DSG2 in xenograft tumors, because in tumors, not all DSG2 is trapped in junctions.[19] (ii) As expected, serum IgG antibodies against JO-4 developed after 1 week. However, the concentration of anti-JO-4 antibodies was at a level that was completely saturated after the second JO-4 injection (no detectable anti-JO-4 antibodies at 4 hours after the second injection). Serum antibodies had no effect on the pharmacokinetics of JO-4 after the second injection. Corresponding JO-4/anti-JO-4 IgG immune complexes were found by ELISA and immunofluorescence analysis of tissue sections in a series of lymphoid (spleen, lymph nodes) and non-lymphoid organs (adrenals, epididymis, lung, kidney, gall bladder, and pancreas). (iii) Nonopsonized JO-4 was detected (at concentrations less than 50 ng per 100 mg tissue) in adrenals, epididymis, lung, liver, and kidneys. (iv) JO-4 pretreatment resulted in a longer Doxil retention in the blood. Depositions of Doxil were found in the liver, adrenals, brain, bone marrow, lymph nodes, and spleen. The most notable effect of JO-4 was that Doxil concentrations were higher in the liver of the JO-4 pretreated animal, while lower Doxil concentrations were found in adrenals, bone marrow, heart, lymph nodes, seminal vesicle, and spleen. We speculate that JO-4 increases the liver's capacity to trap Doxil so that other tissues are less exposed. Clearly, this needs to be validated in more animals. Based on these findings, in the next IND-enabling toxicology study with clinical grade JO-4, we plan to test whether accumulative toxicity develops after four cycles of treatment given at an interval of 4 weeks (based in the design of the clinical trial). We will pay specific attention to adrenals and liver functions. After JO-4 injection into patients, even if they receive chemotherapy with immunosuppressive effects, serum antibodies will develop. In this context, it is noteworthy that anti-JO-4 antibodies generated after injection into immunocompetent mice appeared not to critically inhibit the ability of JO4 to enhance Doxil therapy.[22] In the clinical trial, as a precaution to prevent opsonization of JO-4, we consider treatment with prednisolone for 48 hours before JO-4 injection to suppress anti-JO-4 antibodies.[37]

In summary, our studies in DSG2 transgenic mice and NHPs did not show critical JO-4-related toxicity. These data together with favorable FDA comments to a recently submitted pre-IND application create a basis for a successful clinical application of the JO-4 technology. Our current efforts are focused on the cGMP production of a JO-4 protein in which the His tag has been removed and a large scale GLP-toxicology study in NHPs.

MATERIALS AND METHODS

Proteins

Recombinant human DSG2 protein was from Leinco Technologies (St. Louis, MO). JO-4 was produced in *E. coli* with an N-terminal 6-His tags, using the pQE30 expression vector (Qiagen, Valencia, CA) and purified by Ni-NTA agarose chromatography as described elsewhere.[38] JO-4 preparations used in animals were depleted of bacterial endotoxin using Endotrap blue 1/1 columns (Hyglos GmbH, Bernried, Germany).

Cell lines

Ovc316 cells are Her2/neu-positive epithelial tumor cells derived from an ovarian cancer biopsy.[39] Ovc316 cells were cultured in mammary epithelial cell growth medium (MEGM) (Lonza, Mapleton, IL), containing 3 µg/l hEGF, 5 µg/l insulin, 5 mg/l hydrocortisone, 26 mg/l bovine pituitary extract, 25 mg/l amphotericin B and supplemented with 1% fetal bovine serum, 100 I.U. penicillin, 100 µg/l streptomycin, 10 mg/l ciprofloxacin. MDA-MB-231-luc-D3H2LN cells (Caliper Life Sciences, Hopkinton, MA), a triple-negative breast cancer cell line, were cultured in Leibovitz's L-15 medium supplemented with 10% fetal bovine serum, 100 I.U. penicillin, 100 µg/l streptomycin.

Surface plasmon resonance

Acquisitions were done on a BIAcore 3000 instrument. 0.1 M HEPES, 1.5 M NaCl and 0.05% v/v Surfactant P20 (HBS-P) (GE-Healthcare, Pittsburgh, PA) supplemented with 2 mmol/l $CaCl_2$ was used as running buffer at a flow rate of 15 µl/minute. Immobilization on CM5 sensorchip (BIAcore) was performed using JO-4 at 10 µg/ml diluted in 10 mmol/l Acetate buffer pH 4.5 injected for 10 minutes on ethyl(dimethylaminopropyl) carbodiimide (EDC)/N-Hydroxysuccinimide (NHS) activated flow-cell (7.500 RU). A control flow-cell was activated by (EDC/NHS) and inactivated by ethanolamine. Different concentrations of DSG2 (12.5–200 nmol/l) were injected for 3 minutes of association followed by 2.5 minutes of dissociation time, and the signal was automatically subtracted from the background of the ethanolamine deactivated EDC-NHS flow cell. Regeneration was done by a two-time injection of ethylenediaminetetraacetic acid 10 mmol/l for 2 minutes. Kinetic and affinity constants were calculated using the BIAeval software.

Crystallography

Crystallization conditions for HAdV3 fiber knob mutant V239D were screened using the service of the High Throughput Screening Lab at Hauptman Woodward Medical Research Institute. For diffraction studies, V239D mutant protein was crystallized using the hanging drop method. Crystals were grown using a reservoir solution of 1.75M $MgSO_4(7H_20)$ in TAPS buffer 0.1 mol/l pH9.0 and a protein solution of 8 mg/ml. Crystals were frozen using a cryoprotectant composed of 85% reservoir and 15% glycerol (v/v). Data collection was performed at 100K on an ID23-2 (ref. 40) of the European Synchrotron Radiation Facility (ESRF) using the EDNA-diffraction characterisation and data collection strategy (EDNA) pipeline.[41] Data were indexed and scaled using XDS/XSCALE[42,43] and the structure solved by molecular replacement (PDB 1H7Z) with the program PHASER.[44] The model was built and refined using COOT[45] and BUSTER,[46] respectively. The entry "Structure of the adenovirus 3 knob domain V239D mutant" has been assigned the PDB ID code 4WYJ.

Animal studies

All experiments involving animals were conducted in accordance with the institutional guidelines set forth by the University of Washington.

Mice

Mice were housed in specific-pathogen-free facilities. Immunodeficient (CB17) mice (*st*rain name: NOD.CB17-Prkdc^{scid}/J) were obtained from the Jackson Laboratory (Bar Harbor, ME). Human DSG2 transgenic mice contain 90 kb of the human DSG2 locus and express hDSG2 at a level and in a pattern similar to humans.[20] MDA-MB-231-luc-D3H2LN and ovc316 xenograft tumors were established by injection of the corresponding tumor cells into the mammary fat pad (1:1 with Matrigel) of CB17 mice. JO-4 was intravenously injected one hour before the application of PEGylated liposomal doxorubicin/Doxil (Be Venue Laboratories, Bedford, OH), Tumor volumes were measured three times a week. Each treatment group consisted of a minimum of five mice. Animals were sacrificed and the experiment terminated when tumors in one of the groups reached a volume of 800 mm^3 or tumors displayed ulceration.

In vivo imaging

In vivo luciferase imaging was performed on a IVIS Lumina Series II (PerkinElmer, Waltham, MA). Mice with MDA-MB-231-luc-D3H2LN tumors were imaged as follows: Animals were injected i.p. with 15 mg/ml Luciferin in PBS at 150 mg/kg. Five minutes later, animals were transferred to anesthesia

induction chamber and animals were induced for 3 minutes. Animals were then transferred to the *in vivo* imaging system (IVIS) imaging chamber. Ten minutes after substrate injection, the imaging procedure was started. Two sequences of 5×1 minute exposures were recorded at small binning and F-stop of 1. For the first sequence the primary tumor site was shielded, for the second sequence the shielding was removed. For analysis, regions of interest (ROIs) were put over the primary tumor site and the metastatic site (remainder of the mouse body) and the total flux (photons per second summed over the area of the ROI) of the ROIs was measured using Living Image 4.0 Software (PerkinElmer).

Human DSG2 western blot

Primary tumors and mesenteric metastatic lesions were collected and homogenized in PBS with protease inhibitors (Roche, Mannheim, Germany) with a QIAGEN TissueRuptor (Qiagen). Homogenates were sonicated on ice for 30 seconds and then spun down at 4 °C at maximum speed in a table top centrifuge for 20 minutes. Samples in reducing Laemmli buffer were separated via sodium dodecyl sulfate polyacrylamide gel electrophoresis and blots were incubated with primary anti-human DSG2 (AbD Serotec, Raleigh, NC, 6D8, 1:1,000) and anti-human β-actin (Sigma) (1:3,000) antibodies and a horse radish peroxidase (HRP)-linked secondary anti-mouse IgG antibody (1:2,000).

Macaques

All studies were performed by the Washington State Northwest Primate Research Center at the University of Washington. JO-4 and Doxil (Ben Venue Laboratories, Beford, OH) were infused intravenously at a rate of 2 ml/minute. Blood samples were drawn at the time points indicated. At the end of the observation period, a complete necropsy was performed on selected animals.

Preparation of tissues for ELISA

Hundred milligrams of tissues in PBS-0.05%Tween20 were homogenized using the TissueRuptor system (Qiagen), sonicated for 20 seconds, and subjected to three freeze/thaw cycles. Cell debris was spun down and supernatants from lysed tissues were used in the JO-4 and Doxil ELISA at 1:5, 1:20, and 1:100 dilutions. Two independent tissue samples were used.

DSG2 ELISA

ELISA was performed using the goat polyclonal anti-DSG2 antibody AF947 (R&D Systems, Minneapolis, MN) and the mouse monoclonal antibody 6D8 directed against ECD3 (AbD Serotec, Raleigh, NC). The detection limit of the DSG2 ELISA was 0.5 ng/ml. The antibodies cross-react with macaque DSG2.

JO-4 ELISA

The ELISA consisted of a polyclonal rabbit antibody directed against the HAdV3 fiber knob as capture antibody and a mouse monoclonal anti-HAdV3 fiber knob antibody (clone 2-1) as detection antibody. The sensitivity of the ELISA was 0.5 ng/ml.

Anti-JO-4 antibody ELISA

Polyclonal HAdV3 fiber antibody was absorbed on ELISA plates followed by JO-4 protein at a saturating concentration. Dilutions of monkey serum (1:10, 1:100, and 1,000) were added and binding was detected with either goat-anti monkey IgG+IgA+IgM-HRP (MyBioSource, San Diego, CA).

Doxil ELISA

To measure liposomal doxorubicin/Doxil concentrations, mice were sacrificed and blood was flushed from the circulation with 10 ml PBS. Tissues were homogenized in PBS/0.1% Tween 20/protease inhibitors. Anti-PEG (PEG, polyethylene glycol) antibody AGP4 was used as a capture antibody.[27] Binding was detected with anti-PEG antibody 3.3.-biotin followed by a streptavidin–HRP conjugate.

IFNγ ELISA

Serum interferon-γ levels were measured using an ELISA kit from Invitrogen (Grand Island, NY).

DSG2 Immunofluorescence

The following antibodies were used on 4% para-formaldehyde-fixed OCT sections: anti-PEG mAb-AGP3-biotin[27]; anti-HAdV3 fiber knob mAb- clone 2-1; goat-α-human DSG2 (R&D Systems); anti-monkey IgG-FITC, Non-human Primate Reagent Resource Cat#: 1B3-FITC.

CONFLICT OF INTEREST

A.L. and D.C. are co-owners of Compliment Corp., a start-up company that is involved in the clinical development of the JO-4 technology.

ACKNOWLEDGMENTS

The work was supported by NIH grants R01 CA080192 (A.L.), R01 HLA078836 (A.L.), and the Pacific Ovarian Cancer Research Consortium/Specialized Program of Research Excellence in Ovarian Cancer Grant P50 CA83636 (NU), a grant from Department of Defense (W81XWH-12-1-0600) (A.L.), a grant from BRIM Biotechnology, Inc and a grant from Samyang Biopharmaceuticals Corporation. The NHP studies were supported by the National Primate Research Center at the University of Washington, NIH grant RR00166 and the National Center for Research Resources and the Office of Research Infrastructure Programs (ORIP) of the National Institutes of Health through Grant Number OD 010425. M.R. is a recipient of a fellowship award from the Deutscher Akademischer Austauschdienst (DAAD). We would like to acknowledge the beam line staff on 23-2 at European Synchrotron Radiation Facility (ESRF). We thank Alexandra Sova for help with organizing the NHP data.

REFERENCES

1. Lipinski, CA, Lombardo, F, Dominy, BW and Feeney, PJ (2001). Experimental and computational approaches to estimate solubility and permeability in drug discovery and development settings. *Adv Drug Deliv Rev* **46**: 3–26.
2. Lavin, SR, McWhorter, TJ and Karasov, WH (2007). Mechanistic bases for differences in passive absorption. *J Exp Biol* **210**(Pt 15): 2754–2764.
3. Green, SK, Karlsson, MC, Ravetch, JV and Kerbel, RS (2002). Disruption of cell-cell adhesion enhances antibody-dependent cellular cytotoxicity: implications for antibody-based therapeutics of cancer. *Cancer Res* **62**: 6891–6900.
4. Biedermann, K, Vogelsang, H, Becker, I, Plaschke, S, Siewert, JR, Höfler, H *et al.* (2005). Desmoglein 2 is expressed abnormally rather than mutated in familial and sporadic gastric cancer. *J Pathol* **207**: 199–206.
5. Harada, H, Iwatsuki, K, Ohtsuka, M, Han, GW and Kaneko, F (1996). Abnormal desmoglein expression by squamous cell carcinoma cells. *Acta Derm Venereol* **76**: 417–420.
6. Beyer, I, Cao, H, Persson, J, Song, H, Richter, M, Feng, Q *et al.* (2012). Coadministration of epithelial junction opener JO-1 improves the efficacy and safety of chemotherapeutic drugs. *Clin Cancer Res* **18**: 3340–3351.
7. Turley, EA, Veiseh, M, Radisky, DC and Bissell, MJ (2008). Mechanisms of disease: epithelial-mesenchymal transition–does cellular plasticity fuel neoplastic progression? *Nat Clin Pract Oncol* **5**: 280–290.
8. Christiansen, JJ and Rajasekaran, AK (2006). Reassessing epithelial to mesenchymal transition as a prerequisite for carcinoma invasion and metastasis. *Cancer Res* **66**: 8319–8326.
9. Jolly, MK, Huang, B, Lu, M, Mani, SA, Levine, H and Ben-Jacob, E (2014). Towards elucidating the connection between epithelial-mesenchymal transitions and stemness. *J R Soc Interface* **11**: 20140962.
10. Lu, M, Jolly, MK, Levine, H, Onuchic, JN and Ben-Jacob, E (2013). MicroRNA-based regulation of epithelial-hybrid-mesenchymal fate determination. *Proc Natl Acad Sci USA* **110**: 18144–18149.
11. Choi, IK, Strauss, R, Richter, M, Yun, CO and Lieber, A (2013). Strategies to increase drug penetration in solid tumors. *Front Oncol* **3**: 193.
12. Tannock, IF, Lee, CM, Tunggal, JK, Cowan, DS and Egorin, MJ (2002). Limited penetration of anticancer drugs through tumor tissue: a potential cause of resistance of solid tumors to chemotherapy. *Clin Cancer Res* **8**: 878–884.
13. Minchinton, AI and Tannock, IF (2006). Drug penetration in solid tumours. *Nat Rev Cancer* **6**: 583–592.
14. Fessler, SP, Wotkowicz, MT, Mahanta, SK and Bamdad, C (2009). MUC1* is a determinant of trastuzumab (Herceptin) resistance in breast cancer cells. *Breast Cancer Res Treat* **118**: 113–124.
15. Oliveras-Ferraros, C, Vazquez-Martin, A, Cufí, S, Queralt, B, Báez, L, Guardeño, R *et al.* (2011). Stem cell property epithelial-to-mesenchymal transition is a core transcriptional network for predicting cetuximab (Erbitux™) efficacy in KRAS wild-type tumor cells. *J Cell Biochem* **112**: 10–29.
16. Lee, CM and Tannock, IF (2010). The distribution of the therapeutic monoclonal antibodies cetuximab and trastuzumab within solid tumors. *BMC Cancer* **10**: 255.
17. Wang, H, Li, ZY, Liu, Y, Persson, J, Beyer, I, Möller, T *et al.* (2011). Desmoglein 2 is a receptor for adenovirus serotypes 3, 7, 11 and 14. *Nat Med* **17**: 96–104.

18. Lu, ZZ, Wang, H, Zhang, Y, Cao, H, Li, Z, Fender, P *et al.* (2013). Penton-dodecahedral particles trigger opening of intercellular junctions and facilitate viral spread during adenovirus serotype 3 infection of epithelial cells. *PLoS Pathog* **9**: e1003718.
19. Beyer, I, van Rensburg, R, Strauss, R, Li, Z, Wang, H, Persson, J *et al.* (2011). Epithelial junction opener JO-1 improves monoclonal antibody therapy of cancer. *Cancer Res* **71**: 7080–7090.
20. Wang, H, Beyer, I, Persson, J, Song, H, Li, Z, Richter, M *et al.* (2012). A new human DSG2-transgenic mouse model for studying the tropism and pathology of human adenoviruses. *J Virol* **86**: 6286–6302.
21. Wang, H, Li, Z, Yumul, R, Lara, S, Hemminki, A, Fender, P *et al.* (2011). Multimerization of adenovirus serotype 3 fiber knob domains is required for efficient binding of virus to desmoglein 2 and subsequent opening of epithelial junctions. *J Virol* **85**: 6390–6402.
22. Wang, H, Yumul, R, Cao, H, Ran, L, Fan, X, Richter, M *et al.* (2013). Structural and functional studies on the interaction of adenovirus fiber knobs and desmoglein 2. *J Virol* **87**: 11346–11362.
23. Gordon, AN, Granai, CO, Rose, PG, Hainsworth, J, Lopez, A, Weissman, C *et al.* (2000). Phase II study of liposomal doxorubicin in platinum- and paclitaxel-refractory epithelial ovarian cancer. *J Clin Oncol* **18**: 3093–3100.
24. Muggia, FM, Hainsworth, JD, Jeffers, S, Miller, P, Groshen, S, Tan, M *et al.* (1997). Phase II study of liposomal doxorubicin in refractory ovarian cancer: antitumor activity and toxicity modification by liposomal encapsulation. *J Clin Oncol* **15**: 987–993.
25. Markman, M, Kennedy, A, Webster, K, Peterson, G, Kulp, B and Belinson, J (2000). Phase 2 trial of liposomal doxorubicin (40 mg/m(2)) in platinum/paclitaxel-refractory ovarian and fallopian tube cancers and primary carcinoma of the peritoneum. *Gynecol Oncol* **78**(3 Pt 1): 369–372.
26. Strauss, R, Li, ZY, Liu, Y, Beyer, I, Persson, J, Sova, P *et al.* (2011). Analysis of epithelial and mesenchymal markers in ovarian cancer reveals phenotypic heterogeneity and plasticity. *PLoS One* **6**: e16186.
27. Su, YC, Chen, BM, Chuang, KH, Cheng, TL and Roffler, SR (2010). Sensitive quantification of PEGylated compounds by second-generation anti-poly(ethylene glycol) monoclonal antibodies. *Bioconjug Chem* **21**: 1264–1270.
28. Gusella, M, Bononi, A, Modena, Y, Bertolaso, L, Franceschetti, P, Menon, D *et al.* (2014). Age affects pegylated liposomal doxorubicin elimination and tolerability in patients over 70 years old. *Cancer Chemother Pharmacol* **73**: 517–524.
29. Latifi, A, Abubaker, K, Castrechini, N, Ward, AC, Liongue, C, Dobill, F *et al.* (2011). Cisplatin treatment of primary and metastatic epithelial ovarian carcinomas generates residual cells with mesenchymal stem cell-like profile. *J Cell Biochem* **112**: 2850–2864.
30. Baribeau, S, Chaudhry, P, Parent, S and Asselin, É (2014). Resveratrol inhibits cisplatin-induced epithelial-to-mesenchymal transition in ovarian cancer cell lines. *PLoS One* **9**: e86987.
31. Durmort, C, Stehlin, C, Schoehn, G, Mitraki, A, Drouet, E, Cusack, S *et al.* (2001). Structure of the fiber head of Ad3, a non-CAR-binding serotype of adenovirus. *Virology* **285**: 302–312.
32. Scheel, C and Weinberg, RA (2012). Cancer stem cells and epithelial-mesenchymal transition: concepts and molecular links. *Semin Cancer Biol* **22**: 396–403.
33. Pesonen, S, Nokisalmi, P, Escutenaire, S, Särkioja, M, Raki, M, Cerullo, V *et al.* (2010). Prolonged systemic circulation of chimeric oncolytic adenovirus Ad5/3-Cox2L-D24 in patients with metastatic and refractory solid tumors. *Gene Ther* **17**: 892–904.
34. Koski, A, Kangasniemi, L, Escutenaire, S, Pesonen, S, Cerullo, V, Diaconu, I *et al.* (2010). Treatment of cancer patients with a serotype 5/3 chimeric oncolytic adenovirus expressing GMCSF. *Mol Ther* **18**: 1874–1884.
35. Kim, KH, Dmitriev, I, O'Malley, JP, Wang, M, Saddekni, S, You, Z *et al.* (2012). A phase I clinical trial of Ad5.SSTR/TK.RGD, a novel infectivity-enhanced bicistronic adenovirus, in patients with recurrent gynecologic cancer. *Clin Cancer Res* **18**: 3440–3451.
36. Hemminki, O, Diaconu, I, Cerullo, V, Pesonen, SK, Kanerva, A, Joensuu, T *et al.* (2012). Ad3-hTERT-E1A, a fully serotype 3 oncolytic adenovirus, in patients with chemotherapy refractory cancer. *Mol Ther* **20**: 1821–1830.
37. Dykes, AC, Walker, ID, Lowe, GD and Tait, RC (2001). Combined prednisolone and intravenous immunoglobulin treatment for acquired factor VIII inhibitors: a 2-year review. *Haemophilia* **7**: 160–163.
38. Wang, H, Liaw, YC, Stone, D, Kalyuzhniy, O, Amiraslanov, I, Tuve, S *et al.* (2007). Identification of CD46 binding sites within the adenovirus serotype 35 fiber knob. *J Virol* **81**: 12785–12792.
39. Strauss, R, Sova, P, Liu, Y, Li, ZY, Tuve, S, Pritchard, D *et al.* (2009). Epithelial phenotype confers resistance of ovarian cancer cells to oncolytic adenoviruses. *Cancer Res* **69**: 5115–5125.
40. Flot, D, Mairs, T, Giraud, T, Guijarro, M, Lesourd, M, Rey, V *et al.* (2010). The ID23-2 structural biology microfocus beamline at the ESRF. *J Synchrotron Radiat* **17**: 107–118.
41. Incardona, MF, Bourenkov, GP, Levik, K, Pieritz, RA, Popov, AN and Svensson, O (2009). EDNA: a framework for plugin-based applications applied to X-ray experiment online data analysis. *J Synchrotron Radiat* **16**(Pt 6): 872–879.
42. Kabsch, W (2010). Integration, scaling, space-group assignment and post-refinement. *Acta Crystallogr D Biol Crystallogr* **66**(Pt 2): 133–144.
43. Kabsch, W (2010). XDS. *Acta Crystallogr D Biol Crystallogr* **66**(Pt 2): 125–132.
44. McCoy, AJ, Grosse-Kunstleve, RW, Adams, PD, Winn, MD, Storoni, LC and Read, RJ (2007). Phaser crystallographic software. *J Appl Crystallogr* **40**(Pt 4): 658–674.
45. Emsley, P, Lohkamp, B, Scott, WG and Cowtan, K (2010). Features and development of Coot. *Acta Crystallogr D Biol Crystallogr* **66**(Pt 4): 486–501.
46. Bricogne, G, Brandl, M, Flensburg, C, Keller, P, Paciorek, W, Roversi, P, *et al. BUSTER Version 2.10.0*. Global Phasing Ltd, Cambridge, UK, 2011.

Supplementary Information accompanies this paper on the *Molecular Therapy—Methods & Clinical Development* website (http://www.nature.com/mtm)